with aberrant transcriptional properties[17] cause semidominant human Pallister–Hall (PHS) and post-axial polydactyly (PAP-A) syndromes, which respectively result in medial and post-axial polydactyly[17,30]. Semidominant group 2 mutant alleles function in the context of intact Shh signalling and a normal *Gli3* allele, and thus group 2 mutations collectively present a heterogeneous spectrum of phenotypes. However, group 2 phenotypes are characterized by a lack of mirror-image digit duplications, and affected digits are nearly always syndactylous. Therefore, the position and identity (or lack thereof) of supernumerary digits resulting from different group 2 mutations may vary, and presumably reflects how particular mutations alter the transcriptional output of Gli3-regulated target genes. □

Methods

Animals

The generation and identification of *Shh* and *Gli3* mutant mice were performed as described[22].

Staining and whole-mount *in situ* hybridization

Alcian blue and alizarin red staining of cartilage and bone, and whole mount *in situ* hybridization analyses, were performed as described[22].

Antibody production and western analysis

Amino-terminal-specific GLI3 antibodies were generated against amino acids 396–500 of human GLI3. Fusion proteins of GLI3 and glutathione *S*-transferase (GST) were expressed by *Escherichia coli*, isolated and used to immunize rabbits, according to standard protocols. Antiserum was affinity purified using GST–GLI3 fusion proteins immobilized on Affi-gel 10 beads (Bio-Rad). We collected 150 μg of protein lysate samples from anterior and posterior limb bud halves, and resolved them on 7.5% SDS–polyacrylamide gels. Using anti-N-terminal GLI3 (1: 400) primary antibodies and biotinylated anti-rabbit immunoglobulin-γ secondary antibodies, we visualized protein bands by incubation with a streptavidin-peroxidase conjugate followed by an enhanced chemiluminescence detection method (Amersham).

Received 12 April; accepted 2 August 2002; doi:10.1038/nature01033.
Published online 18 August 2002.

1. Ingham, P. W. & McMahon, A. P. Hedgehog signaling in animal development: paradigms and principles. *Genes Dev.* **15,** 3059–3087 (2001).
2. Masuya, H., Sagai, T., Wakana, S., Moriwaki, K. & Shiroishi, T. A duplicated zone of polarizing activity in polydactylous mouse mutants. *Genes Dev.* **9,** 1645–1653 (1995).
3. Büscher, D., Bosse, B., Heymer, J. & Rüther, U. Evidence for genetic control of *Sonic hedgehog* by *Gli3* in mouse limb development. *Mech. Dev.* **62,** 175–182 (1997).
4. Wang, B., Fallon, J. F. & Beachy, P. A. Hedgehog-regulated processing of Gli3 produces an anterior/posterior repressor gradient in the developing vertebrate limb. *Cell* **100,** 423–434 (2000).
5. Méthot, N. & Basler, K. Hedgehog controls limb development by regulating the activities of distinct transcriptional activator and repressor forms of Cubitus interruptus. *Cell* **96,** 819–831 (1999).
6. Méthot, N. & Basler, K. An absolute requirement for Cubitus interruptus in Hedgehog signaling. *Development* **128,** 733–742 (2001).
7. Aza-Blanc, P., Ramirez-Weber, F. A., Laget, M. P., Schwartz, C. & Kornberg, T. B. Proteolysis that is inhibited by Hedgehog targets Cubitus interruptus protein to the nucleus and converts it to a repressor. *Cell* **89,** 1043–1053 (1997).
8. Pearse, R. V. & Tabin, C. J. The molecular ZPA. *J. Exp. Zool.* **282,** 677–690 (1998).
9. Yang, Y. *et al.* Relationship between dose, distance and time in *Sonic hedgehog*-mediated regulation of anteroposterior polarity in the chick limb. *Development* **124,** 4393–4404 (1997).
10. Lewis, P. M. *et al.* Cholesterol modification of Sonic hedgehog is required for long-range signaling activity and effective modulation of signaling by Ptc1. *Cell* **105,** 599–612 (2001).
11. Chiang, C. *et al.* Manifestation of the limb prepattern: Limb development in the absence of Sonic hedgehog function. *Dev. Biol.* **236,** 421–435 (2001).
12. Kraus, P., Fraidenraich, D. & Loomis, C. A. Some distal limb structures develop in mice lacking Sonic hedgehog signaling. *Mech. Dev.* **100,** 45–58 (2001).
13. Sanz-Ezquerro, J. J. & Tickle, C. "Fingering" the vertebrate limb. *Differentiation* **69,** 91–99 (2001).
14. Dai, P. *et al.* Sonic hedgehog-induced activation of the *Gli*1 promoter is mediated by GLI3. *J. Biol. Chem.* **274,** 8143–8152 (1999).
15. Brewster, R., Lee, J. & Ruiz i Altaba, A. Gli/Zic factors pattern the neural plate by defining domains of cell differentiation. *Nature* **393,** 579–583 (1998).
16. Brewster, R., Mullor, J. L. & Ruiz i Altaba, A. Gli2 functions in FGF signaling during antero-posterior patterning. *Development* **127,** 4395–4405 (2000).
17. Shin, S. H., Kogerman, P., Lindstrom, E., Toftgard, R. & Biesecker, L. G. GLI3 mutations in human disorders mimic *Drosophila* Cubitus interruptus protein functions and localization. *Proc. Natl Acad. Sci. USA* **96,** 2880–2884 (1999).
18. Sasaki, H., Nishizaki, Y., Hui, C.-c., Nakafuku, M. & Kondoh, H. Regulation of Gli2 and Gli3 activities by an amino-terminal repression domain: implication of Gli2 and Gli3 as primary mediators of Shh signaling. *Development* **126,** 3915–3924 (1999).
19. Hui, C. C. & Joyner, A. L. A mouse model of Greig cephalopolysyndactyly syndrome: the *extra-toes*^{J} mutation contains an intragenic deletion of the *Gli3* gene. *Nature Genet.* **3,** 241–246 (1993).
20. Zúñiga, A. & Zeller, R. *Gli3 (Xt)* and *formin (ld)* participate in the positioning of the polarising region and control of posterior limb-bud identity. *Development* **126,** 13–21 (1999).
21. te Welscher, P., Fernandez-Teran, M., Ros, M. A. & Zeller, R. Mutual genetic antagonism involving GLI3 and dHAND prepatterns the vertebrate limb bud mesenchyme prior to SHH signaling. *Genes Dev.* **16,** 421–426 (2002).
22. Litingtung, Y. & Chiang, C. Specification of neuronal cell types in the ventral spinal cord is mediated by antagonistic interaction between Shh and Gli3. *Nature Neurosci.* **3,** 979–985 (2000).
23. Caruccio, N. C. *et al.* Constitutive activation of Sonic hedgehog signaling in the chicken mutant *talpid*^{2}: Shh-independent outgrowth and polarizing activity. *Dev. Biol.* **212,** 137–149 (1999).
24. Martin, G. R. The roles of FGFs in the early development of vertebrate limbs. *Genes Dev.* **12,** 1571–1586 (1998).
25. Zúñiga, A., Haramis, A.-P. G., McMahon, A. & Zeller, R. Signal relay by BMP antagonism controls the SHH/FGF4 feedback loop in vertebrate limb buds. *Nature* **401,** 598–602 (1999).
26. Sun, X. *et al.* Conditional inactivation of Fgf4 reveals complexity of signalling during limb bud development. *Nature Genet.* **25,** 83–86 (2000).
27. Fraidenraich, D., Lang, R. & Basilico, C. Distinct regulatory elements govern Fgf4 expression in the mouse blastocyst, myotomes, and developing limb. *Dev. Biol.* **204,** 197–209 (1998).
28. Castilla, E. E. *et al.* Epidemiological analysis of rare polydactylies. *Am. J. Med. Genet.* **65,** 295–303 (1996).
29. Qu, S. *et al.* Polydactyly and ectopic ZPA formation in *Alx-4* mutant mice. *Development* **124,** 3999–4008 (1997).
30. Radhakrishna, U. *et al.* The phenotypic spectrum of Gli3 morphopathies includes autosomal dominant preaxial polydactyly type IV and postaxial polydactyly type A/B. *Am. J. Hum. Genet.* **65,** 645–655 (1999).

Supplementary Information accompanies the paper on *Nature*'s website (http://www.nature.com/nature).

Acknowledgements

We thank Y.-F. Wang, R. Mernaugh and J. Lancman for technical assistance; R. Harland and B. Vogelstein for reagents; and S. Carroll and members of the Fallon laboratory for critical comments on the manuscript. This work was supported by grants from the National Institutes of Health to C.C. and J.F.F.

Competing interests statement

The authors declare that they have no competing financial interests.

Correspondence and requests for materials should be addressed to C.C. (e-mail: chin.chiang@vanderbilt.edu) or J.F.F. (e-mail: jffallon@facstaff.wisc.edu).

T-cell engagement of dendritic cells rapidly rearranges MHC class II transport

Marianne Boes*, Jan Cerny†‡§, Ramiro Massol†‡ Marjolein Op den Brouw*, Tom Kirchhausen†‡, Jianzhu Chen‖ & Hidde L. Ploegh*

** Department of Pathology,*
† The Center for Blood Research, and
‡ Department of Cell Biology, Harvard Medical School, 200 Longwood Avenue, Boston, Massachusetts 02115, USA
‖ Center for Cancer Research and Department of Biology, Massachusetts Institute of Technology, 40 Ames Street, Cambridge, Massachusetts 02139, USA
§ Faculty of Science, Charles University, Albertov 6, Prague, van Černy, Czech Republic

Assembly of major histocompatibility complex (MHC) molecules, which present antigen in the form of short peptides to T lymphocytes, occurs in the endoplasmic reticulum; once assembled, these molecules travel from the endoplasmic reticulum to their final destination. MHC class II molecules follow a route that takes them by means of the endocytic pathway, where they acquire peptide, to the cell surface[1]. The transport of MHC class II molecules in 'professional' antigen-presenting cells (APCs) is subject to tight control and responds to inflammatory stimuli such as lipopolysaccharide. To study class II transport in live APCs, we replaced the mouse MHC class II gene with a version that codes for a class II molecule tagged with enhanced green fluorescent protein (EGFP). The resulting mice are immunologically indistinguishable from wild type. In bone-marrow-

derived dendritic cells, we observed class II molecules in late endocytic structures with transport patterns similar to those in Langerhans cells observed *in situ*. We show that tubular endosomes extend intracellularly and polarize towards the interacting T cell, but only when antigen-laden dendritic cells encounter T cells of the appropriate specificity. We propose that such tubulation serves to facilitate the ensuing T-cell response.

To visualize transport of class II MHC molecules in live APCs, we generated mice in which the endogenous class II product is replaced by a fluorescently tagged version, through germline manipulation. We replaced the $I\text{–}A^b\beta$ gene in J1 (129/Sv; H–2^b) embryonic stem (ES) cells with a construct encoding a protein composed of an intact class II β-chain fused at its carboxy terminus with an EGFP moiety (Fig. 1a). One homologous integrant embryonic stem cell clone was obtained and used to derive germline knock-in mice, identified by fluorescence-activated cell sorting (FACS) screening of I–A^b EGFP-positive B cells in peripheral blood (data not shown). Knock-in mice, but not wild-type animals, showed the presence of an anti-EGFP-reactive polypeptide of the expected size, 56K (relative molecular mass (M_r) of 56,000; Fig. 1b). No free EGFP (27K) was detected. Thus, EGFP visualized by microscopy represents MHC class II molecules tagged with EGFP (MHC II-EGFP).

Maturation of MHC class II molecules, monitored by pulse-chase analysis and digestion with endoglycosidase H, occurs normally in MHC II-EGFP mice. The rate of acquisition of endoglycosidase H resistance is indistinguishable for MHC class II molecules and the EGFP-tagged class II molecules (data not shown). The diagnostic presence of SDS-resistant dimers—a surrogate marker for peptide occupancy—indicates that peptide loading proceeds with similar kinetics in heterozygous and in homozygous MHC II-EGFP mice (Fig. 1c).

The expression of MHC products is a prerequisite for development of an appropriately restricted T-cell repertoire[2,3]. Flow cytometry of thymus and lymph node showed normal production of $CD4^+$ and $CD8^+$ T cells in MHC II-EGFP mice (Fig. 1d). We found no significant differences in serum immunoglobulin levels between the wild-type and knock-in mice (Fig. 1e). The MHC II-EGFP fusion protein therefore allows APCs to stimulate the CD4 T-cell populations required for immunoglobulin class switching.

We generated dendritic cells from MHC II-EGFP mice using bone marrow cultures supplemented with granulocyte/macrophage-colony stimulating factor (GM-CSF) and interleukin (IL)-4. At day 5, yields of dendritic cells and marker profiles (CD11b, CD11c, CD80, CD86, MHC class II) were indistinguishable from wild-type littermates (data not shown). Such dendritic cells expressed low to intermediate levels of CD86, and MHC II-EGFP was contained almost entirely intracellularly. There is a strict requirement for the activation of dendritic cells, notably by microbial products such as lipopolysaccharide (LPS), in order to achieve strong surface expression of MHC class II molecules[22]. Indeed, treatment of

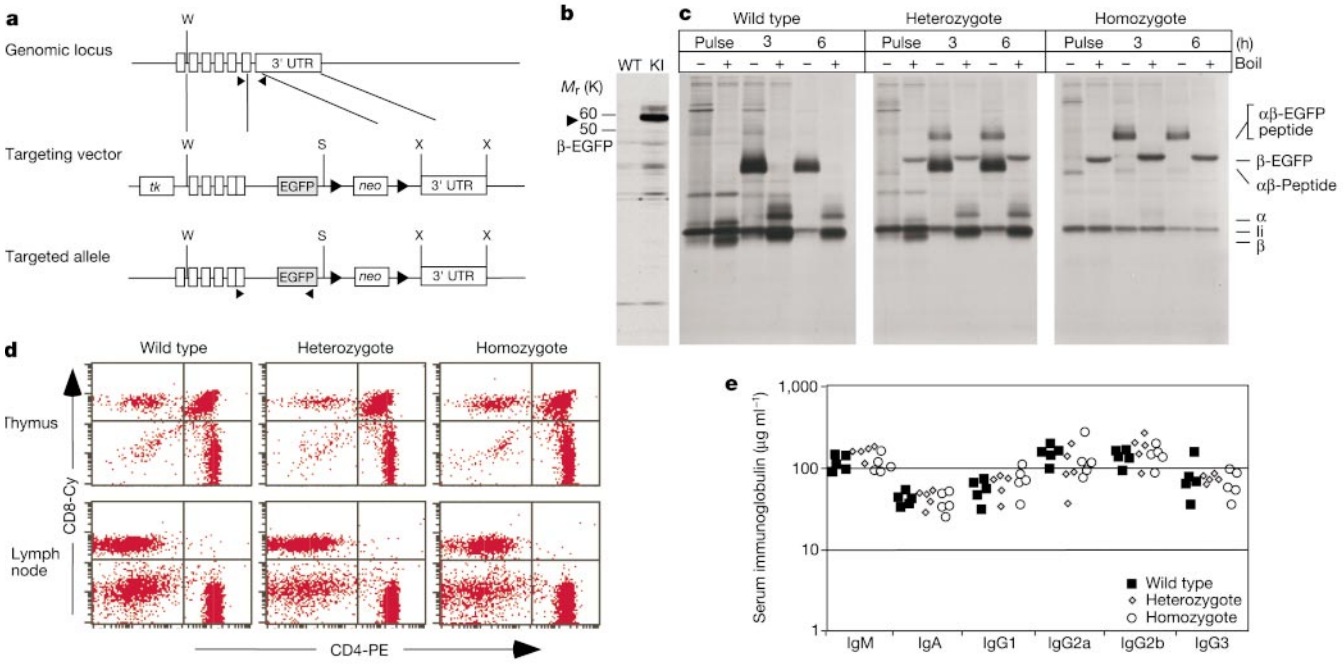

Figure 1 Generation and characterization of MHC II-EGFP knock-in mice. **a**, I–Aβ-EGFP knock-in mice (H–2^b background) were generated by replacing the β-chain gene with β-EGFP via homologous recombination in ES cells. The genomic sequence encoding exons 2–6 were used as the 5′ homologous region. The 3′ untranslated region was used as the 3′ homologous region, obtained by PCR from genomic DNA. The targeting vector consisted of a floxed (triangles) phosphoglycerate kinase promoter-driven neomycin (*neo*) resistance gene, flanked by a 4.8-kb *SwaI*/*SalI* (S) homologous fragment upstream and by a 1.6-kb *XbaI*/*Xba*I (X) homologous fragment downstream. As a marker for counter selection, the thymidine kinase (*tk*) gene was placed upstream from the 5′ homologous region. Sequences encoding exons 5 and 6 were ligated together using a linker sequence (5′- TCGATTGTCGACATTTAAATCTCGAGGCCCTCCTCCAGCAGGACTCCTGCAG-3′). **b**, Whole spleen cell lysates were separated by 12.5% SDS–PAGE and transferred to PVDF membranes. Membranes were blotted using a polyclonal anti-EGFP antibody generated against bacterially expressed EGFP; arrowhead indicates position of fusion protein. WT, wild type; KI, knock-in. **c**, Splenocytes were pulse-labelled for 45 min with 0.5 mCi ml^{-1} [^{35}S]methionine/cysteine and chased in complete DMEM for 3 and 6 h. Class II molecules were recovered by immunoprecipitation with the N22 antibody. Immunoprecipitates were re-suspended in sample buffer containing 5% 2-ME, either boiled or kept on ice for 5 min, and analysed by 12.5% SDS–PAGE. Ii, invariant chain. **d**, T-cell populations in knock-in mice analysed by flow cytometry. Single-cell suspensions prepared from thymus and lymph node were stained with conjugated antibodies and analysed by FAC-Scan (Becton Dickinson). Percentages of CD4 T cells are: thymus, 27.4%, 27.5% and 38.8%; lymph node, 51.6%, 52.9% and 58.7% for wild-type, heterozygous and homozygous knock-in animals, respectively. Percentages of CD8 T cells are: thymus, 7.6%, 5.5% and 8.7%; lymph node, 23.6%, 28.4% and 15.8% for wild-type, heterozygous and homozygous knock-in animals, respectively. **e**, Serum immunoglobulin levels determined by ELISA from 6-week-old littermates. Each symbol represents a serum sample from one mouse.

dendritic cells with LPS led to a redistribution of MHC II-EGFP molecules to the plasma membrane (Fig. 2d, right panel).

In dendritic cells we observed extensive co-localization of MHC II-EGFP with internalized DiI-labelled low-density lipoprotein (LDL), a protein targeted ultimately for lysosomal destruction (See Supplementary Information 1 and ref. 4). In contrast, there was little apparent co-localization of Alexa Fluor 594-labelled transferrin with MHC II-EGFP (Fig. 2a). Thus, the class II-positive structures are not readily accessible to tracers that mark early and recycling endocytic compartments. We then exposed dendritic cells to *Salmonella typhimurium* expressing the red fluorescent protein DsRed1. After 3 h, internalized bacteria did not show appreciable co-localization with MHC II-EGFP (Fig. 2b), but after 5 h each intracellular bacterium resided in a compartment positive for MHC II-EGFP (Fig. 2c). Combined, these data establish that MHC II-EGFP molecules reside primarily in late endocytic compartments.

Intracellular movement of MHC II-EGFP-positive compartments was quite dynamic (see also ref. 5), as changes in location can be observed in confocal images captured only seconds apart. EGFP-positive compartments are vesicular and tubular structures, with tubules showing the most dynamic movement (Fig. 2d). These tubules are up to approximately 5 μm in length, move at speeds up to 2 μm s^{-1} (Supplementary Information 2d) and may be similar to those reported in D1 cells exposed for several hours to LPS[6]. This transport of class II-positive compartments is strictly microtubule-dependent. Within 8 min of application of the microtubule-disrupting agent nocodazole, class II-EGFP-positive tubules are no longer visible in the more distal projections of the cells. After 40 min of nocodazole treatment, all MHC class II molecules had collapsed to a location close to the nucleus (Supplementary Information 2).

Langerhans cells are regarded as prototypic immature dendritic cells localized in the epidermis. In fixed tissue sections, Langerhans cells are strongly positive for MHC class II molecules (ref. 7). We examined the distribution of MHC II-EGFP in fresh epidermal sheets prepared from mouse ears. A three-dimensional reconstruction of an isotropic set of 50 confocal images shows the distribution of Langerhans cells within the epidermis (Fig. 3a). We found that MHC II-EGFP is localized primarily to the central portion of the cell, with well-demarcated vesicles present in the more remote extensions, giving the appearance of beads on a string. Intracellular movement of class II-positive compartments can be observed *in situ* even in these preparations (Fig. 3b).

We next studied the fate of class II-containing compartments in dendritic cells on contact with T cells. We pulsed dendritic cells with either hen egg lysozyme (HEL) or ovalbumin (Ova) overnight and removed excess antigen by washing. Under these circumstances, display at the cell surface of peptide-loaded MHC molecules will occur. We then added the HEL-specific T hybridoma 46.13 (HEL, residues 46–61; I–A^b restricted)[8], or the Ova-specific T hybridoma B097.1 (Ova, residues 323–339; I–A^b restricted)[9]. Randomly selected dendritic cell–T-cell conjugates were then analysed immediately by time-lapse confocal microscopy (Fig. 4a, b). Contacts between T cells and dendritic cells resulted in immediate (within minutes) and pronounced tubulation of class II-positive compartments, such that a tubule (usually one or two per cell) would point directly to the area of contact between a dendritic cell and a T cell. These tubules reached extraordinary lengths, at times exceeding 50 μm, and emanated from the large accumulation of MHC II-EGFP around the microtubule-organizing centre. Both the kinetics of tubulation and the length of tubules formed are quite different from those seen in the D1 cell line exposed to LPS[6]. Where several T cells interacted with a single dendritic cell, tubules extended to each of the interacting T cells. Tubules of much reduced length and of no preferred orientation were observed when dendritic cells had not encountered antigen, yet were exposed to antigen-specific T cells in the same manner (data not shown; see also Fig. 5). Samples examined at later times (2 and 6 h after addition of antigen-specific T cells) still contained such extended tubular class II-positive compartments in 55–75% of dendritic cells exposed to antigen, but in fewer than 5% of dendritic cells loaded with the wrong antigen or with no antigen at all. Three-dimensional reconstructions performed on fixed dendritic cell–T-cell conjugates showed the presence of MHC II-EGFP-positive tubules laid down on a lattice of microtubules (Fig. 4c), which was again disrupted by nocodazole (data not shown).

Primary T cells obtained from the lymph nodes of OTII T-cell

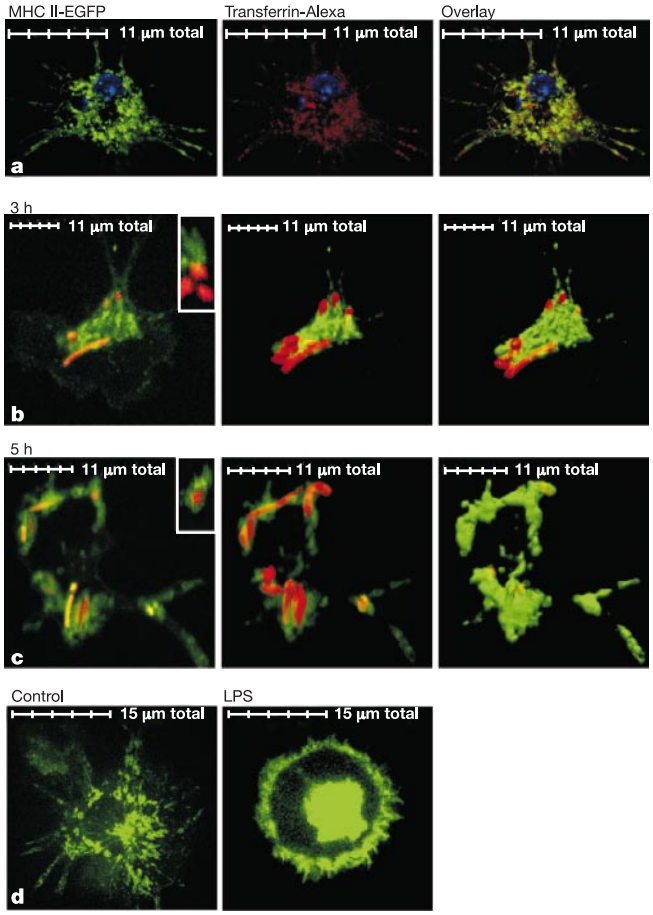

Figure 2 MHC II-EGFP molecules in dendritic cells reside in late endosomes. **a**, Dendritic cells (day 5 of culture) were allowed to endocytose transferrin labelled with Alexa Fluor 594 for 30 min, and were then immediately visualized in a single optical section by time-lapse confocal microscopy. Nuclei (blue) are visualized by incubation with Hoechst 33258 (15 min at 37 °C). **b**, Dendritic cells (day 5) were allowed to endocytose live *S. typhimurium* expressing DsRed1 for 1 h. Unbound bacteria were washed away, and dendritic cells were analysed by confocal microscopy after a total of 3 h (left). Inset, magnification of a cross-section taken perpendicular to the confocal image. *S. typhimurium* is close to, but not enveloped by, a MHC II-$EGFP^+$ compartment (middle). After 3 h, bacteria are taken up by dendritic cells, but do not reside in MHC II-$EGFP^+$ compartments (right). **c**, After 5 h of exposure, most *S. typhimurium* are enveloped within MHC II-$EGFP^+$ compartments. Dendritic cells were analysed by confocal microscopy (left). Inset, magnification of a cross-section taken perpendicular to the confocal plane shown in the larger image. *S. typhimurium* is surrounded by a MHC II-$EGFP^+$ compartment. By rendering the green fluorescence either transparent (middle) or opaque (right), the complete engulfment of *S. typhimurium* at 5 h is apparent. At 5 h, degradation of bacteria commences, as in some vesicles the DsRed1-labelled bacteria appear as round rather than rod-like structures. **d**, Day 4 dendritic cells were either left untreated (left) or were treated with 5 μg ml^{-1} LPS overnight (right) and visualized the next day by confocal microscopy in a single optical section. LPS activation induced morphological changes and increased display of class II molecules on the cell membrane (right).

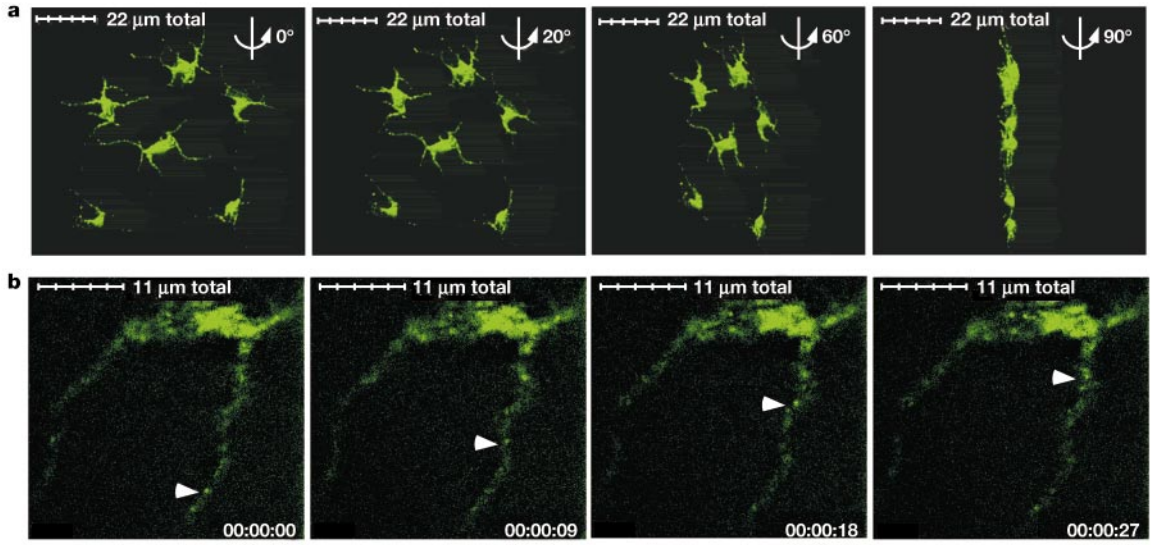

Figure 3 Transport of MHC II-EGFP-containing structures in Langerhans cells *in situ*. **a**, Langerhans cells on the epidermal sheet were visualized by three-dimensional volume renditions of 50 confocal microscopy images. **b**, Examination of a single Langerhans cell in a whole mount by time-lapse microscopy in a single optical section. Vesicular movement is apparent, as evident from the tracking of a single vesicle (arrowhead).

antigen receptor (I–A^b restricted, Ova-specific) transgenic mice (Fig. 5) evoked similar extensive tubulation (again, one to two extended tubules per cell) when confronted with Ova-loaded, but not control, dendritic cells (Fig. 5c). A quantification of the length, orientation and particularly the frequency of the polarized tubules aimed at the T cell (Fig. 5b, category 1 tubules) illustrates the marked response elicited by naive OTII T cells when cognate antigen is present. OTII T cells exposed to antigen-laden dendritic cells upregulated CD69, but not when Ova was withheld (Fig. 5a). Activation of naive OTII T cells thus correlates with the antigen-dependent occurrence of the tubulation induced by them.

The availability of mice that express EGFP-tagged MHC class II

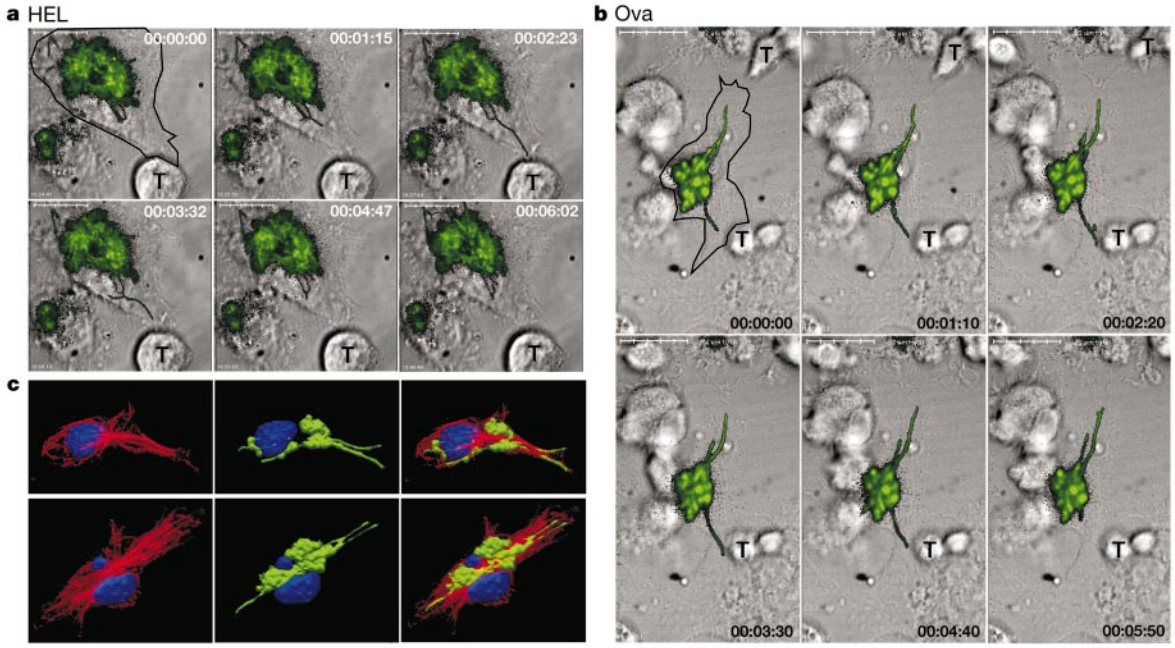

Figure 4 Microtubule-driven directional transport of endosomal compartments on T-cell contact. **a**, Day 4 dendritic cells cultured on coverslips at 1×10^6 per well (six-well plate) and incubated with 300 μM HEL (Sigma) overnight to induce display of HEL-peptide on class II molecules on the cell membrane. T hybridoma cells specific for HEL(46–61) peptide were brought into contact with dendritic cells by a 30-s centrifugation step (see Methods). Time-lapse confocal microscopy in a single optical section was performed immediately after imposition of contact, and at 2 and 6 h thereafter (not shown), yielding most MHC II-EGFP tubuli after 2 and 6 h. Scale bar, 13 μm. **b**, As in **a**, except that dendritic cells were incubated with 300 μM Ova and T hybridoma cells specific to OVA(323–339) were used. Most MHC II-EGFP tubuli were revealed after 2 and 6 h. A T cell in the upper right quadrant is moving out of the field of view between 2.20 and 3.30 min, whereas a T cell in the lower right corner is stationary for the time observed. Scale bar, 22 μm. **c**, T hybridoma cells specific for HEL(46–61) peptide were added to HEL-loaded dendritic cells and were cultured for an additional 2 h at 37 °C to induce tubulation of MHC II-$EGFP^+$ compartments. Dendritic cell/T-cell clusters were fixed in 3% paraformaldehyde, and microtubuli were visualized by staining for α-tubulin (red, labelled with Cy3, nuclei are stained blue; see Methods).

molecules has allowed us to visualize the transport of class II MHC molecules in live cells. The use of a knock-in approach ensures balanced levels of expression of the MHC II-EGFP reporter in the appropriate cell types. Moreover, it allows an *in vivo* validation of the functionality of the EGFP-tagged class II molecules by examining mice homozygous for the knock-in mutation. This is important, because even non-professional APCs such as fibroblasts can be rendered capable of antigen presentation and T-cell stimulation by simple transfection with class II complementary DNAs[10], yet few would argue that such cells should be considered representative of professional APCs.

Having established that MHC II-EGFP mice are phenotypically normal, the knock-in mice were used as a source of bone marrow from which dendritic cells could be cultured by providing GM-CSF and IL-4 growth factors. On contacting an APC, T cells form supramolecular activation clusters, or SMACs, also referred to as the immunological synapse[11,12]. Our results indicate marked changes in subcellular organization in the APC also: tubular endosomes that contain abundant class II molecules are aimed directly at the interacting T cell in a strictly antigen-dependent manner (Figs 4 and 5). Such rearrangement may maximize delivery of peptide-loaded class II molecules to the T cell. Models for T-cell activation prominently include a requirement for multiple sequential interactions for the T cell to surpass the threshold indicative of a productive interaction with the APC[13–15]. The ability of a dendritic cell to direct and sustain delivery of class II peptide complexes to site(s) at which the interactions with T cells occur would assist in generating a productive signal. Prolonged interaction (hours) between dendritic cells and T cells may be required to obtain full activation[16]. How can the initial dendritic cell–T-cell contact be used to maximize delivery of MHC peptide complexes to the responding T cell? Our observations suggest that directed transport of class II molecules from intracellular stores to the T-cell contact site(s) may provide the solution.

There may well be a link between the ligation of class II molecules at the surface, caused by contact with an antigen-specific T cell, and the ensuing polarization towards the contact interface. Specifically, the activation of protein kinase C occurs on ligation of surface class II molecules[17]. For such signalling to be possible, some small number of the appropriate peptide–MHC complexes would have to be present. Further recruitment of class II molecules from intracellular stores would follow by tubulation on T-cell contact. If, as we suspect, the rearrangement of the class II transport pathway increases a T cell's probability of receiving appropriate stimulation, then microbes could target this process as a means of immune evasion. Many bacteria have co-opted the host cytoskeleton as essential for their survival or contributing to virulence. It would not seem far-fetched, then, to suggest interference with tubulation as a possible escape mechanism. □

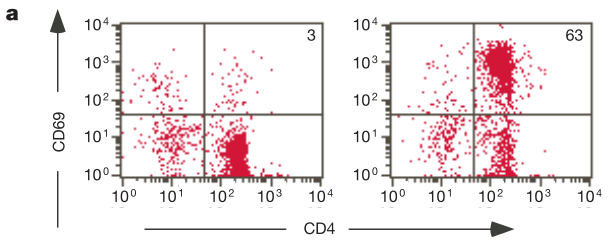

No antigen

Class	(Av. length (μm))
1	4.6 ± 2.2 (*n* = 13)
2	4.8 ± 3.0 (*n* = 20)
3	4.6 ± 2.9 (*n* = 39)

Conjugates with no tubules: 21
Number of conjugates: 53

Ovalbumin

Class	(Av. length (μm))
1	21.4 ± 11.9 (*n* = 70)
2	13.3 ± 10.4 (*n* = 19)
3	9.6 ± 5.9 (*n* = 15)

Conjugates with no tubules: 0
Number of conjugates: 51

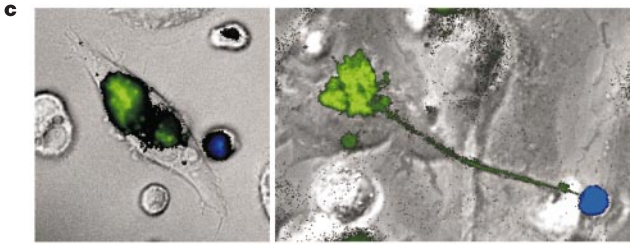

Figure 5 Primary T cells induce tubulation in dendritic cells in an antigen-dependent manner. **a**, Analysis of T-cell activation by expression of the CD69 marker. OTII T cells (lymph node) were exposed to antigen-pulsed dendritic cells (day 5) for 18 h and analysed by cytofluorimetry for CD4 and CD69 markers. Numbers in the upper-right quadrant indicate cell percentage in the quadrant. **b**, Quantitative analysis of tubulation induced by OTII cells. Naive OTII T cells were labelled with Hoechst 33258 and incubated with dendritic cells (day 5) in the absence or presence of Ova (200 μM, 18 h). OTII T cells were added to the coverslips on which dendritic cells were grown and conjugate formation was initiated by a brief centrifugation. Images were captured in epifluorescence mode. Tubules that extended directly towards the interacting T cell were classified as '1', those that included a vector towards the interacting T cell, but not pointing directly at the T cell, were classified as '2', and tubules pointing away from the interacting T cell were classified as '3' (top). For some conjugates, more than one tubule extending towards the T cell was observed. In the absence of antigen, a conjugate was defined as a dendritic cell touched by a T cell. Numbers of conjugates, numbers of tubules, mean values for tubule length and s.d. are given. *t*-test analysis of the tubules classified as Ova-treated compared with untreated dendritic cells yields the *P*-values: 1, $P < 0.0001$; 2, $P < 0.0001$; 3, $P = 0.0002$. **c**, Tubulation in the absence and presence of Ova. Superposition of the bright-field image, green fluorescence (dendritic cells) and blue fluorescence (T cell) is shown. The left panel shows tubulation in the absence of Ova; tubulation in the presence of Ova is shown in the right panel. The length of the MHC class II^+ tubule is 41 μm. Images were taken 3 h after addition of T cells.

Methods

Targeting vector and mutant mice

To produce a mutant mouse strain carrying an EGFP label on all MHC β-chains, we made use of an ES cell line, J1, which was derived from a 129/Sv mouse. This strain is b-haplotype at the H–2 locus and therefore carries a mutation in the *E*α gene promoter that precludes synthesis of Eα protein, and therefore prevents expression of cell surface I–E complex[18]. The starting material was a 6.3-kilobase (kb) *Eco*RI fragment from an Aβ genomic clone carried in the plasmid pcEXV-n (a gift from D. Mathis).

Western blot

Whole-cell lysates were prepared from 1×10^7 splenocytes by lysis in NP-40 lysis buffer pH 7.4 (50 mM Tris-HCl, 150 mM NaCl, 0.5% NP-40) supplemented with 1% SDS for 30 min on ice. Proteins were separated on SDS–polyacrylamide gel electrophoresis (PAGE) and transferred to polyvinylidene difluoride (PVDF) membranes (NEN Life Science Products). Membranes were blocked with 10% milk in PBS/0.1% Tween, and blotted with a rabbit polyclonal anti-EGFP antibody that was generated by our laboratory.

Pulse-chase analysis and immunoprecipitations

Pulse-chase experiments and immunoprecipitations were performed as described[19]. Briefly, splenocytes were pulsed for 45 min with 0.5 mCi ml^{-1} [^{35}S]methionine/cysteine (Du Pont New England Nuclear) and chased in complete DMEM for 3 and 6 h. After each chase point, cells were lysed in NP-40 lysis buffer at pH 7.4 supplemented with 1% SDS. Class II molecules were recovered by immunoprecipitation with the N22 antibody; a reagent that captures properly folded and assembled class II molecules (N22 was a gift of R. M. Steinman). Immunoprecipitations were carried out with *Staphylococcus aureus*, were washed four times with washing buffer (0.5% NP-40, 50 mM Tris-HCl, pH 7.4, 150 mM NaCl, 5 mM EDTA), resuspended in sample buffer containing 5% 2-ME, either boiled or kept on ice for 5 min, and analysed by SDS–PAGE.

Flow cytometry analyses

CD4 and CD8 T-cell development in the knock-in mice was analysed by flow cytometry.

Phycoerythrin- and cychrome-conjugated monoclonal antibodies specific for CD4 and CD8 were from PharMingen. Single-cell suspensions were prepared from thymus and lymph node. Ten thousand live cells were collected for each sample.

Enzyme-linked immunosorbent assay (ELISA)

We measured serum immunoglobulin levels by ELISA (Southern Biotechnology Associates). Plates were coated with goat anti-mouse immunoglobulin-μ, -γ and -α and developed with horseradish peroxidase-conjugated goat antibodies specific for each mouse immunoglobulin isotype. The concentrations were calculated using the linear ranges of the dilution and purified mouse immunoglobulin isotypes as standards.

Cell preparation and culture

Dendritic cells were generated as described[20]. Briefly, cells were flushed from the bone marrow cavity with PBS/2.5% FCS. Cells were plated at 1×10^6 cells per well in 2 ml DMEM, 25 mM HEPES and 10% FCS without phenol red, and 10 ng ml^{-1} GM-CSF and 1 ng ml^{-1} IL-4. Cells were cultured on 25-mm circular coverslips, with changes of medium every second day; non-adherent cells were removed by gentle washing. For activation, LPS (5 μg ml^{-1}) was added for the last 20 h of culture.

Epidermal sheet preparation

Ear snips were obtained from MHC II-EGFP mice, and hairs were removed using an epilating agent (Nair, Carter Products). Epidermal sheets were generated by separation of ear snips into dorsal and ventral halves, with the use of forceps.

Imaging of MHC II-EGFP molecules in dendritic cells

We used 5-day-old bone marrow dendritic cells for real-time imaging. For dissection of early and late endocytic compartments, dendritic cells were incubated with 25 μg ml^{-1} transferrin Alexa Fluor 594 (Molecular Probes) or DiI-LDL (10 μg ml^{-1}; provided by M. Krieger) for 30 min at 37 °C in DMEM without serum and washed three times. Similarly, dendritic cells were incubated with DsRed1-labelled (Clontech) *S. typhimurium* (provided by M. Starnbach) in normal medium without penicillin/streptomycin for 1 h, and analysed after a total of 3–5 h. Images were captured with an inverted Zeiss 200M microscope equipped with a ×63 objective (1.4NA PanApo) and a spinning-wheel confocal head (Perkin-Elmer), and supplied with a 37 °C open perfusion temperature-controlled chamber (20/20 Technology). We used Slidebook (Intelligent Imaging Innovation Inc) for image acquisition and data processing. Volocity (Improvision Inc) was used for creating a three-dimensional rendition of the volume.

Antigen presentation in real time

Dendritic cells at a concentration of 1×10^6 per coverslip were incubated with 300 μM HEL or Ova (Sigma) to induce display of antigen-derived peptides on class II molecules. Dendritic cells were then washed three times with culture medium. T cells (0.5×10^6) were labelled with the nuclear dye Hoechst 33258 (Molecular Probes), washed and then added to each coverslip containing dendritic cells. The HEL-specific T-cell hybridoma used was H46.13, which is specific for HEL(46–61) (provided by C. Alfonso); the Ova-specific T-cell hybridoma was B097.1, which is specific for Ova(323–339) (provided by P. Marrack). Freshly isolated Ova-specific OTII T cells were obtained from lymph nodes from OTII transgenic mice[21]. T cells were brought into contact with dendritic cells by a quick centrifugation step at 600 *g*. at room temperature. Confocal microscopy analysis was performed immediately after 2 and 6 h.

Immunostaining of fixed dendritic cells

Five-day-old dendritic cells on coverslips were fixed in 3% paraformaldehyde in PBS, 1 mM Mg^{2+} and 0.1 mM Ca^{2+} (PBS-MC) for 10 min at 37 °C. Dendritic cells were washed extensively with PBS-MC and were permeabilized for 10 min with 0.5% saponin in PBS-MC at room temperature. Dendritic cells were washed and any excess of reactive groups of paraformaldehyde were quenched with 50 mM NH4Cl in PBS-MC for 15 min at room temperature. Anti-α tubulin (1:100, Oxford Biotechnology) staining was done in PBS-MC overnight at 4 °C. We used a rat anti-mouse Cy3-labelled secondary antibody for detection (Jackson Immunoresearch).

Received 4 April; accepted 3 July 2002; doi:10.1038/nature01004.

1. Villadangos, J. A. *et al.* Proteases involved in MHC class II antigen presentation. *Immunol. Rev.* **172,** 109–120 (1999).
2. Cosgrove, D. *et al.* Mice lacking MHC class II molecules. *Cell* **66,** 1051–1066 (1991).
3. Grusby, M. J., Johnson, R. S., Papaioannou, V. E. & Glimcher, L. H. Depletion of CD4 + T cells in major histocompatibility complex class II-deficient mice. *Science* **253,** 1417–1420 (1991).
4. Brown, M. S. & Goldstein, J. L. A receptor-mediated pathway for cholesterol homeostasis. *Science* **232,** 34–47 (1986).
5. Wubbolts, R. *et al.* Direct vesicular transport of MHC class II molecules from lysosomal structures to the cell surface. *J. Cell Biol.* **135,** 611–622 (1996).
6. Kleijmeer, M. *et al.* Reorganization of multivesicular bodies regulates MHC class II antigen presentation by dendritic cells. *J. Cell Biol.* **155,** 53–63 (2001).
7. Rowden, G. The Langerhans cell. *Crit. Rev. Immunol.* **3,** 95–180 (1981).
8. Maric, M. *et al.* Defective antigen processing in GILT-free mice. *Science* **294,** 1361–1365 (2001).
9. Hugo, P., Kappler, J. W., Godfrey, D. I. & Marrack, P. C. A cell line that can induce thymocyte positive selection. *Nature* **360,** 679–682 (1992).
10. Malissen, B., Steinmetz, M., McMillan, M., Pierres, M. & Hood, L. Expression of I-Ak class II genes in mouse L cells after DNA-mediated gene transfer. *Nature* **305,** 440–443 (1983).
11. Monks, C. R., Freiberg, B. A., Kupfer, H., Sciaky, N. & Kupfer, A. Three-dimensional segregation of supramolecular activation clusters in T cells. *Nature* **395,** 82–86 (1998).
12. Grakoui, A. *et al.* The immunological synapse: a molecular machine controlling T cell activation. *Science* **285,** 221–227 (1999).
13. Valitutti, S., Muller, S., Cella, M., Padovan, E. & Lanzavecchia, A. Serial triggering of many T-cell receptors by a few peptide-MHC complexes. *Nature* **375,** 148–151 (1995).
14. Underhill, D. M., Bassetti, M., Rudensky, A. & Aderem, A. Dynamic interactions of macrophages with T cells during antigen presentation. *J. Exp. Med.* **190,** 1909–1914 (1999).
15. Gunzer, M. *et al.* Antigen presentation in extracellular matrix: interactions of T cells with dendritic cells are dynamic, short lived, and sequential. *Immunity* **13,** 323–332 (2000).
16. Lanzavecchia, A. & Sallusto, F. Regulation of T cell immunity by dendritic cells. *Cell* **106,** 263–266 (2001).
17. Scholl, P. R. & Geha, R. S. MHC class II signalling in B-cell activation. *Immunol. Today* **15,** 418–422 (1994).
18. Mathis, D. J., Benoist, C., Williams, V. E., Kanter, M. & McDevitt, H. O. Several mechanisms can account for defective Eα gene expression in different mouse haplotypes. *Proc. Natl Acad. Sci. USA* **80,** 273–277 (1983).
19. Villadangos, J. A., Riese, R. J., Peters, C., Chapman, H. A. & Ploegh, H. L. Degradation of mouse invariant chain: roles of cathepsins S and D and the influence of major histocompatibility complex polymorphism. *J. Exp. Med.* **186,** 549–560 (1997).
20. Villadangos, J. A. *et al.* MHC class II expression is regulated in dendritic cells independently of invariant chain degradation. *Immunity* **14,** 739–749 (2001).
21. Barnden, M. J., Allison, J., Heath, W. R. & Carbone, F. R. Defective TCR expression in transgenic mice constructed using cDNA-based alpha- and beta-chain genes under the control of heterologous regulatory elements. *Immunol. Cell Biol.* **76,** 34–40 (1998).
22. Turley, S. J. *et al.* Transport of peptide-MHC class II complexes in developing dendritic cells. *Science* **288,** 522–527 (2000).

Supplementary Information accompanies the paper on *Nature*'s website (http://www.nature.com/nature).

Acknowledgements

We thank M. Boxem for help in designing the targeting construct and T. Schmidt for blastocyst microinjections. We thank A. W. M. van der Velden for providing DsRed1-labelled *S. typhimurium*, and we acknowledge discussions with members of the Ploegh laboratory.

Competing interests statement

The authors declare that they have no competing financial interests.

Correspondence and requests for materials should be addressed to H.L.P. (e-mail: ploegh@hms.harvard.edu).

Dendritic cell maturation triggers retrograde MHC class II transport from lysosomes to the plasma membrane

Amy Chow, Derek Toomre, Wendy Garrett & Ira Mellman

Department of Cell Biology and Section of Immunobiology, Ludwig Institute for Cancer Research, Yale University School of Medicine, 333 Cedar Street, PO Box 208002, New Haven, Connecticut 06520-8002, USA

Central to the initiation of immune responses is recognition of peptide antigen by T lymphocytes. The cell biology of dendritic cells makes them ideally suited for the essential process of antigen presentation[1]. Their life cycle includes several stages characterized by distinct functions and mechanisms of regulation[2]. Immature dendritic cells synthesize large amounts of major histocompatibility complex class II molecules (MHC II), but the αβ-dimers are targeted to late endosomes and lysosomes (often referred to as MHC class II compartments) where they reside unproductively with internalized antigens. After exposure to microbial products or inflammatory mediators, endocytosis is downregulated, the expression of co-stimulatory molecules is enhanced, and newly formed immunogenic MHC II–peptide complexes are transported to the cell surface[3–10]. That these MHC II molecules reach the surface is surprising, as the lysosomes comprise the terminal degradative compartment of the